厚生労働科学研究費補助金（医療機器開発推進研究事業）
分担研究報告書

ハロゲン化物シンチレータの光物性および放射線応答特性の評価

分担研究者　柳田　健之
東北大学・多元物質科学研究所・助教（研究特任）

研究要旨

本研究の大目標は次世代X線CT用ハロゲン化物シンチレータを開発し、放射線検出器としてのアセンブリを施すことでそのシグナル検出までを目指すものである。該分担ではそのうち、光物性の評価、放射線応答の評価、および放射線検出器プロトタイプの構成までを担った。本年度は真空紫外光を減衰させないように細心の注意を払いながら、光物性・放射線応答評価システムを構築し、評価体制の定常化を行った。加えてガス受光素子を用いた放射線検出器プロトタイプにおいて、ガンマ線の検出に成功し、ダイヤモンド半導体受光素子を用いた同プロトタイプにおいてα線からのシグナル検出に成功した。

A．研究目的

当該分担研究分野の目的は、前段の物質設計、合成、結晶性評価後の物質に対して詳細な光物性評価を行い、強い発光が観測されたものに対しては放射線検出器としてアセンブリし、放射線シグナルの検出を目指すこと、および受光素子としてのガス比例計数管、ダイヤモンド受光素子の開発である。光物性に対する具体的な評価項目としては、シンチレータ結晶の透過スペクトル、発光スペクトル、およびX線励起時における発光スペクトルである。放射線応答の評価に関しては、既存の枯れた技術である光電子増倍管を用いての発光量、蛍光減衰時定数を評価する。真空紫外用の新規受光素子の開発およびその動作検証が目的であるので、最も発光の強い物質群を用いて、保有する放射線源中で最も励起エネルギーの強い ^{241}Am からのα線、もしくは ^{137}Cs からのガンマ線を照射し、そのシグナルの確認を波高値スペクトルにおいて確認することである。

今年度は主に合成されたフッ化物シンチレータに関する光物性評価および放射線特性評価系を確立し、電離性ガス封入型ガス比例計数管受光素子の基礎開発、ダイヤモンド半導体受光素子の基礎開発を行い、ガス比例計数管とCore Valence Luminescence 型シンチレータを融合させた放射線検出器によるガンマ線シグナルの検出、ダイヤモンド受光素子と賦活剤添加型シンチレータをアセンブリした放射線検出器によるα線の信号検出までを行った。

B．研究方法

B-1．光物性評価システム

図1に当該研究で用いた真空紫外域まで感度を有する光物性評価システムの概要を示す。

透過率の評価、Photoluminescence の評価に関し

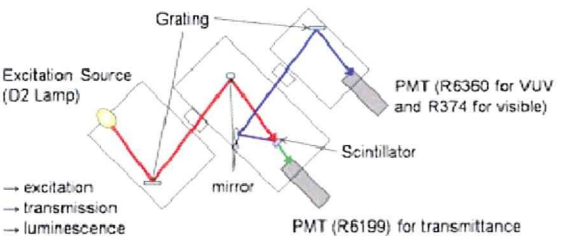

図1 光物性評価システムの概要。

ては励起源として重水素ランプの白色光を用いており、回折格子を用いて波長の単色化を行っている。透過率に関しては真空紫外から可視光までの全波長域に感度を有する浜松ホトニクス社の R6199 型光電子増倍管を用いており、Photoluminescence 用としては真空紫外域に対しては R6360 型、可視光域に対しては R374 型光電子増倍管を用いている。例としてこれらを用いて取得した Nd:LaF_3 結晶の透過率と Photoluminescence スペクトルを図 2 に示す。

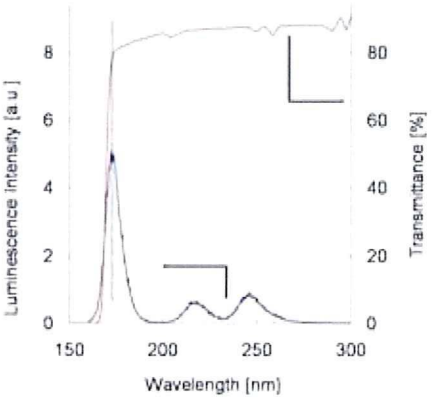

図 2 Nd:LaF_3 シンチレータの発光スペクトルおよび透過スペクトル。

図から明らかなように、当該材料は 170 nm 前後の真空紫外領域まで透過率 80%以上の透明性を有しており、また 173 nm に Nd^{3+}の 5d-4f 遷移に起因する強い発光ピークが見て取れる。X 線励起発光スペクトルもほぼ同様であるが、光励起時に比べて各ラインの強度が変化するなど、ホスト材料から発光中心元素へのエネルギー輸送過程の様子を追うことが可能である。すなわち本評価系でもって、新規に合成した材料の真空紫外域における光物性の評価が可能である。

B-2. 放射線応答評価システム

図 3 には発光量および蛍光減衰時定数を評価するための放射線計測システムの概略を示す。サンプル結晶を VUV 域まで透過性を有する光学接着剤クライトックス 16350 を用いて光電子増倍管 R8778 に光学接着する。ORTEC710 から-1300V の高電圧を印加し、アノードからの出力を、ORTEC572 整形増幅器を通すことでガウス関数型の信号に波形整形し、最後に AD 変換を行うことで PC 等にデータを取り込み、そのパルス波高値を評価することで発光量を求める。また、光電子増倍管からの出力をオシロスコープに取り込むことで蛍光寿命の評価を行う。当該実験系では系統的に 1 ナノ秒弱程度の誤差が見込まれるが、これはシンチレータの蛍光寿命に比べて十分遅いため、無視できる。

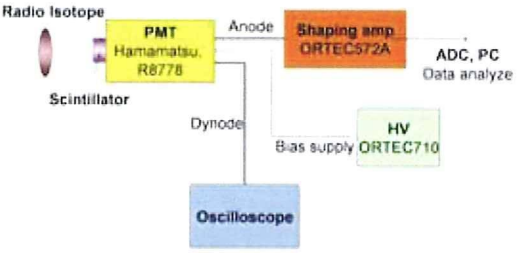

図 3 放射線応答計測システムの概略。

以上の実験系を用いて取得した結果を図 4 に示す。左が蛍光の時間プロファイルであり、蛍光寿命はピークトップから強度が 1/e に減少するまでの時間として定義される。本測定系における Nd:LaF_3 の蛍光寿命はおおよそ 8±1 ナノ秒であり、既存のシンチレータよりも一桁応答が早いことが確認された。右の図は波高値スペクトルである。^{241}Am の照射時のみ、ガウス関数状のピークを示すことが分かり、確かに放射線を検出していることが分かった。Nd:LaF_3 を用いての明確な放射線の検出は、これまで幾多の研究者が達成できなかった世界初の成果であり、本研究において構築した実験系の計測レベルの高さを実証

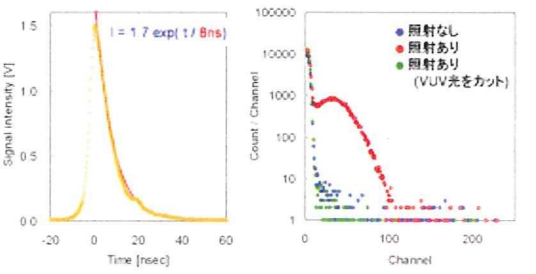

図 4 Nd:LaF3 の蛍光寿命の時間プロファイル(左)および波高値スペクトル(右)。

するものである。単一光電子と比較した場合、Nd:LaF_3 の絶対発光量は 32 phe/5.5MeV α となり、用いた受光素子の量子効率を考慮して、おおよそ 100 光子の発光量を示すことが明らかになった。

B-3. 新規受光素子の開発

本研究では、次世代の高感度な放射線検出器を具現化すべく、従来の光電子増倍管に代替しうる受光素子の開発を目指す。そのための基礎実験として、本年度は真空紫外域にイオン化ポテンシャルを有する電離性ガス封入型ガス比例計数管を開発した。

また、同様に真空紫外域のみに感度を有し、小型・軽量・省電力を同時に実現するダイヤモンド半導体受光素子の開発も行った。ガス比例計数管と異なり、半導体検出器においては I-V、C-V 特性の把握も必須であることから、これらを同時に測定するシステムも立ち上げた。

これらの開発に際して、放射線照射時の信号の読み出し系は結果に関しては図 3 と同様のものを用いており、結果に関しては後述する。

C. 研究結果

C-1. 光物性の評価結果

本研究では、他分担研究者によって得られた結晶すべてに対して光物性特性の測定を行った。測定した結晶のサンプル数は数百種に及ぶため、図 5 にはその一部の結果を示す。図 5-(a)は各種結晶の透過率の様子であり、添加剤ごとに異なる吸収ピークが検出されている。(b)は VUV 光励起における Nd 濃度の異なる LaF_3 シンチレータの発光スペクトルであり、Nd 濃度に依存して発光強度が変化する様子が見受けられる。このように、ひとつの結晶組成に対しても、発光中心元素の置換量を変化させることで特性は大きく変化するため、何種類かの濃度を持つサンプルを合成してみることも必須である。当該評価においては 1%添加が最適であるという結論が得られた。(c)は X 線励起における、Nd 濃度の異なる Nd 添加 BYF の発光スペクトルである。こちらの結果からは、BYF 系結晶においては Nd 添加量は 3%前後が最適であるという結果が得られた。

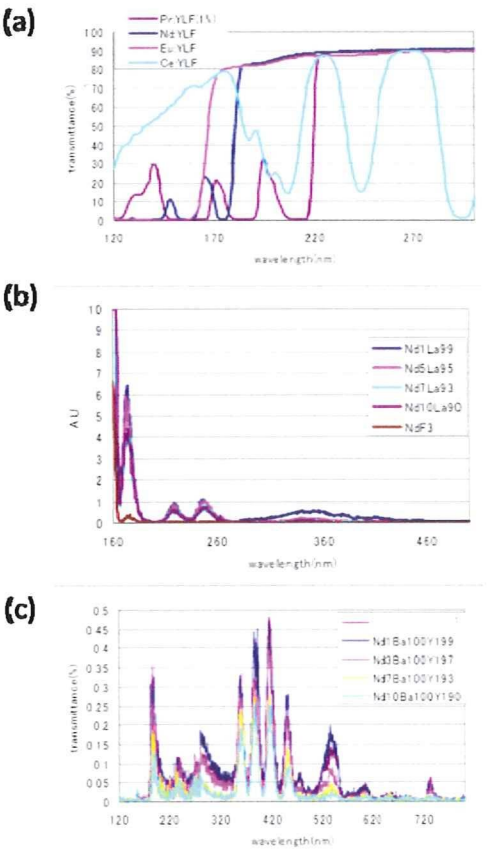

図 5 光物性評価の一例。

C-2. 放射線応答特性の評価結果

光物性評価において、真空紫外域における発光強度が強い結晶に関しては、図 3 の実験系を用いて発光量、蛍光減衰時定数の評価を行った。図 6 には Nd 濃度の異なる $LuLiF_4$ 結晶の波高値スペクトルを示す。照射した線源は ^{241}Am の α 線であり、評価システムのゲイン等はすべて同じである。図にしめしたように、全ての Nd:$LuLiF_4$ 結晶において Nd:LaF_3 の 5-7 倍程度の発光量を示している。結果として、本年度得られた結晶の中で、最大の発光量を示したものは Nd:$LuLiF_4$ 結晶であった。

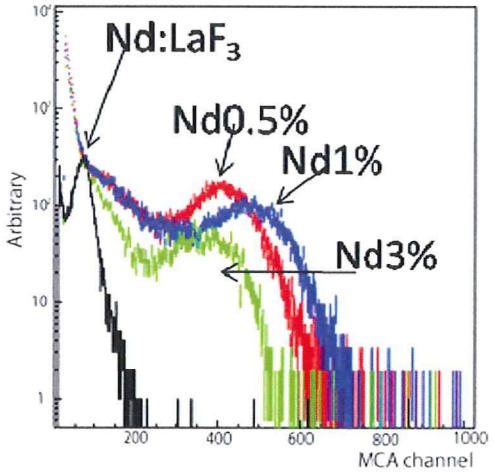

図 6 ^{241}Am 照射時の Nd:LaF_3 および Nd0.5%、1%、3% 添加 $LuLiF_4$ 結晶の波高値スペクトル。

同様のサンプル群における蛍光減衰時定数の比較が図 7 である。一見してわかるように、全てのサンプルが同等の時間プロファイルを示し、蛍光寿命を評価したところ、12 ナノ秒であった。Nd:LaF_3 に比べて数ナノ秒劣るものの、現在発見されているシンチレータにおいては最速の部類に入る値である。

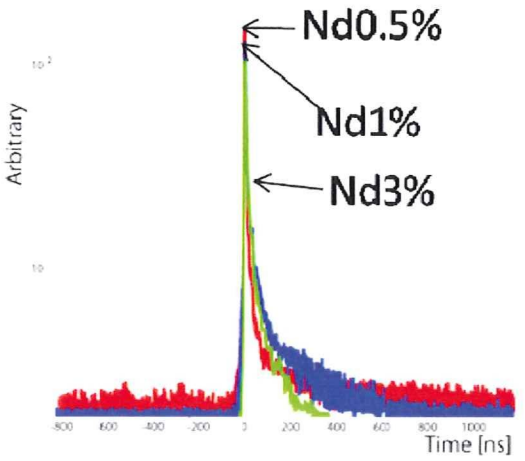

図 7 Nd:$LuLi_4$ 結晶の蛍光寿命時間プロファイル。

以上のような結果が、光物性と同様に数百サンプルに対して得られた。これらの内、最も良い特性を示した Nd:$LuLiF_4$ 結晶に関しては、現在、チョクラルスキー法を用いた高品質大口径化技術の開発を行っている。

C－3．新規受光素子の開発結果

既述のように、新規受光素子としては電離性ガスを封入したガス比例計数管とダイヤモンド半導体受光素子が期待されている。そこで本年度はこれらを放射線検出器における受光素子としての動作検証を中心に行った。図 8 には本研究用に特化して開発した真空紫外光検出用ガス比例計数管受光素子の外観を示す。通常の低エネルギー計測用比例計数管では窓等は付随していないが、本研究にて開発した比例計数管は、真空紫外域においてもっとも高い透過率を持ち、なおかつ放射線励起において励起子からの発光等が存在しないパッシブな材料という観点から MgF_2 窓を有している。内部では 60 μm 径のタングステンワイヤを電極として用いており、3000 V 程度までの高電圧の印加が可能である。

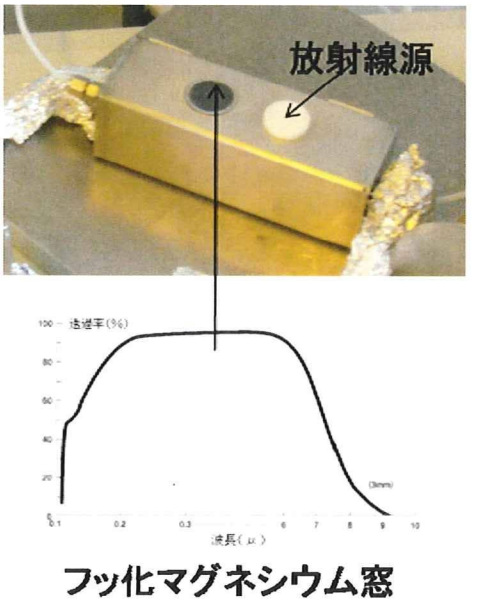

図 8 新規開発した比例計数管受光素子(上)とフッ化マグネシウム窓の透過率(下)。

図 9 には当該実験系を用いた放射線応答の結果を示す。左は TEA と呼ばれる電離性ガスを封入し、^{55}Fe からの 5.9 keV の X 線を直接照射した際の電圧対増幅率のプロットである。一般に比例計数管においては封入ガスの違いに応じて多少の差異は存在するが、電圧を印加、即ち電場勾配を急にすればするほど大

きな雪崩増幅を引き起こすことができる。本結果からも電圧と増幅率の比例関係が見て取れており、すなわち新規開発した比例計数管型受光素子そのものは正しく動作さていることが検証できた。右図は、Core Valence Luminescence による強い発光が有名な $KMgF_3$ 結晶を MgF_2 窓に光学的に接着し、^{137}Cs のガンマ線を照射した際のエネルギースペクトルである。一見してわかるように、平らなノイズ成分上に、特異な形状を持つピークが検出されている。三本のピークはそれぞれ印加電圧値を変化させた場合に対応しており、この位置が変化することから電気的なノイズに由来するものではないことが明らかである。そのため、VUV 発光結晶と比例計数管型受光素子を融合させて放射線検出器は、ガンマ線シグナルの取得までに成功したと言える。原理懸賞フェーズはほぼ完了したことから、現状は単素子であるガス比例計数管受光素子を多素子化することで、次世代 X 線 CT 用の撮像検出器の開発に進みたい。

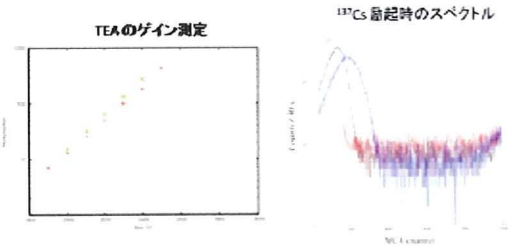

図 9 TEA ガス封入時の増幅率の電圧依存性(左)、および $KMgF_3$ 結晶を用いた際の ^{137}Cs のエネルギースペクトル。

ガス型受光素子と並行し、ダイヤモンド半導体受光素子の検討も行った。そもそも核医学やセキュリティ分野などで用いられている可視光用シンチレータも、1940 年代から 2000 年前後までは光電子増倍管との融合が主流であったが、近年は内部増幅機能を有する Si-APD などの半導体受光素子との融合研究が盛んに行われている。そのため、当該応用においても究極的にはダイヤモンド受光素子の応用に行き着くものと予想し、本研究を行った。図 10 にはダイヤモンド半導体素子と $Nd:LaF_3$ 結晶を用いた検出器プロトタイプ、および該検出器に ^{241}Am の α 線を照射した際の結果を示す。現状は基礎開発であるため、ダイヤモンド半導体素子を何らかの物質で封じきることはせずに、単純にステムで電極を機械的に保護するのみの構造で行っている。このような実験系では、シンチレーション光の収集効率は増すが、一方で酸素による真空紫外光の吸収を防ぐために、窒素パージもしくは真空状態にしたチャンバー中で実験を行わなければならない。左図素子下の円盤状金属は、チャンバーの一部である。シンチレータ、半導体を融合させ、チャンバー内に設置した後は、窒素置換を行い、酸素を極力減らすことが必要となる。そのような状態で ^{241}Am を照射した際のエネルギースペクトルが右図である。一見してわかるように、明らかにノイズとは異なるピークが検出されている。同様の実験を他の結晶に関しても行った結果、幾つかの結晶からは同様の全吸収ピークの検出に成功した。しかしながら、α 線に比べて励起エネルギーが一桁低く、また透過能力が極めて高いガンマ線に関してはいまだ有為な検出に成功してはいない。そこで、次年度の半導体開発における目標としては、ダイヤモンド半導体素子の設計を最適化することで感度を高め、ガンマ線の初検出を目指すこととする。なお、ダイヤモンドを受光素子として動作させ、放射線計測までを行ったのは世界初の成果であるため、興味を示す共同研究企業らと特許出願を行った。

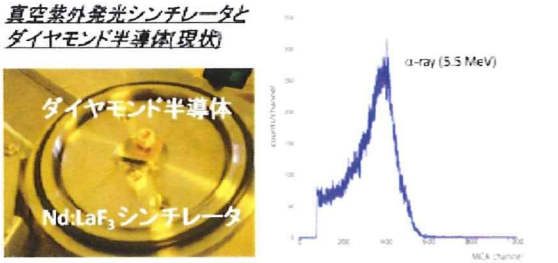

図 10 ダイヤモンド半導体と $Nd:LaF_3$ シンチレータによる次世代放射線計測システムプロトタイプ(左)、および ^{241}Am 照射時のエネルギースペクトル。

D．結論

本年度の研究目標は、

①光物性評価システムの確立

②放射線応答評価システムの確立

③光物性・放射線応答の定常的な評価

④ガス比例計数管受光素子の開発

⑤ダイヤモンド半導体受光素子の開発

であった。

既述の通り、①、②、③に関しては完全に目標を達成し、次年度以降はこれをベースに運用していくこととなる。問題点としては、蛍光寿命における系統誤差が 1 ns 程度生じるために、もしも現状よりも高速なシンチレータが発見された際には対応できないことである。この問題を解決するため、現在、世界初のパルス X 線励起型ストリークカメラを設計中である。

④に関しては、ガンマ線のシグナル検出までに至ったため、目標は達成した。次年度以降は、撮像検出器の開発を目指す。

⑤に関しては、現在α線のシグナル取得までは成功している。次年度以降は引き続きガンマ線のシグナル取得を目指す。

E．健康危険情報

特に無し。

F．研究発表

1. 論文発表

(1) 英文論文

1) T. Yanagida, K. J. Kim, K. Kamada, K. Aoki, N. Kawaguchi, K. Fukuda and A. Yoshikawa, "Measurement of Light Yield of Ce^{3+} Perturbed Emission of CaF_2 Scintillator coupled with Avalanche Photodiode", The Institute of Electrical and Electronics Engineers, Inc. (IEEE NSS/MIC) 2008, N2-357 Conference Record, (2009) 1162-1165.

(2) 和文論文

1) 吉川彰, 柳田健之, 横田有為, 荻野拓, " 新規シンチレータ結晶の開発と放射線検出器としての結実；発光メカニズムの選択から受光素子の選択、アレイ化、アセンブリおよび 2 次元マップの撮像まで" , 日本結晶成長学会誌 35(2) (2008) 17-23.

2) 柳田健之, 河口範明, 横田有為, 石津澄人, 福田健太郎, 藤本裕, 阿部直人, 吉川彰," Ce^{3+}および Pr^{3+} 添加 $YLiF_4$、$BaLiF_3$、$LiCaAlF_6$ 結晶の放射線励起時における発光特性評価" , 第 19 回光物性研究会論文集 (2008) 286-289.

3) 柳田健之, 河口範明, 横田有為, 石津澄人, 福田健太郎, 藤本裕, 阿部直人, 吉川彰: "Ce^{3+}および Pr^{3+} 添加 $YLiF_4$、$BaLiF_3$、$LiCaAlF_6$ 結晶の放射線励起時における発光特性評価" 第 19 回光物性研究会論文集 (2008) 286-289.

2. 学会発表

(1) 国際学会

1) A. Yoshikawa, M. Kimura, C. Kamada, T. Yanagida, Y. Yokota and F. Saito, "Single Crystal Growth and Optical Properties of Pr-doped $K(Y,Lu)_3F_{10}$", Japanese-French Joint Workshop, First Workshop Tohoku University- EMAC- INSA, Ecole des Mines, Albi & INSA,Toulouse, Dec. 1-2. 2008, Albi, France.

2) T. Yanagida, K. J. Kim, K. Kamada, K. Aoki, N. Kawaguchi, K. Fukuda and A. Yoshikawa, "Measurement of Light Yield of Ce^{3+} Perturbed Emission of CaF_2 Scintillator Coupled with APD", The Institute of Electrical and Electronics Engineers, Inc. (IEEE NSS/MIC) 2008, Oct. 19-25. 2008, Dresden, Germany.

3) T. Yanagida, K. J. Kim, K. Kamada, K. Aoki, N. Kawaguchi, K. Fukuda, A. Yoshikawa and F. Saito: "Absolute Light Yield of Ce^{3+} Perturbed Emission in Calcium Fluoride Scintillator", Japanese-French Joint Workshop, First Workshop Tohoku University-EMAC- INSA Ecole des Mines, Albi & INSA, Toulouse, Dec. 1-2. 2008, Albi, France.

4) N. Abe, Y. Yokota, T. Yanagida, N. Kawaguti, F. Nara, A. Yoshikawa and F. Saito, "Crystal Growth and Scintillation Properties of Tm: BaF_2 Single Crystals", Japanese-French Joint Workshop, First Workshop Tohoku University- EMAC- INSA, Ecole des Mines, Albi & INSA,Toulouse, Dec. 1-2. 2008, Albi, France.

5) K. Fukuda, N. Kawaguchi, T. Yanagida, A. Yoshikawa, M. Nikl and F. Saito, "Crystal growth and scintillation property of Nd:LaF_3 single crystal", Japanese-French Joint Workshop, First Workshop Tohoku University-EMAC- INSA, Ecole des Mines, Albi & INSA,Toulouse, Dec. 1-2. 2008, Albi, France.

(2) 国内学会

1) 柳田健之, 横田有為, 鎌田圭, 河口範明, 福田健太郎, 吉川彰," シンチレータおよびその発光波長に適合した受光素子の開発" , 第 69 回応用物理学関係連合講演会 （秋季大会）, 2008 年 9 月 2 日～5

日, 春日井, 中部大学（シンポジウム：招待講演）.

2) 中里智治, 古川裕介, Marilou Cadatal, 清水俊彦, 猿倉信彦, 柳田健之, 福田健太郎, 須山敏尚, 吉川彰, 斎藤文良, " 2 光子吸収過程を利用した Nd^{3+} : LaF_3 からの真空紫外光発生と蛍光寿命評価" , 第 69 回応用物理学関係連合講演会（秋季大会）, 2008 年 9 月 2 日～5 日, 春日井, 中部大学.

3) 阿部直人, 横田有為, 柳田健之, 金敬鎭, 河口範明, 奈良郁子, 吉川彰," Tm 添加 BaF_2 単結晶の作製及びシンチレーション特性評価" , 第 69 回応用物理学関係連合講演会（秋季大会）, 2008 年 9 月 2 日～5 日, 春日井, 中部大学.

4) 柳田健之, 河口範明, 横田有為, 石津澄人, 福田健太郎, 藤本裕, 阿部直人, 吉川彰," Ce^{3+}および Pr^{3+} 添加 $YLiF_4$、$BaLiF_3$、$LiCaAlF_6$ 結晶の放射線励起時における発光特性評価" , 第 19 回　光物性研究会, 2008 年 12 月 5、6 日, 大阪市立大学.

G. 知的財産権の出願・登録状況

1) 発明の名称：「真空紫外発光素子」
発明者：吉川彰, 柳田健之, 横田有為, 福田健太郎, 河口範明, 須山敏尚
出願人：トクヤマ, 東北大学
出願番号：特願 2008-240552
出願日：2008 年 9 月 19 日

2) 発明の名称：「放射線検出装置及び放射線の検出方法」
発明者：吉川彰, 柳田健之, 横田有為, 河口範明, 福田健太郎, 横田嘉宏, 橘武史
出願人：東北大学, トクヤマ, 神戸製鋼所
出願番号：特願 2009-298231
出願日：2009 年 1 月 28 日

研究成果の刊行に関する一覧表

雑誌

発表者氏名	論文タイトル名	発表誌名	巻号	ページ	出版年
A. Yoshikawa, K. Aoki, K. Kamada, F. Saito, M. Itoh, T. Katagiri, D. Iri and M. Fujita	Excitation Energy Transfer in CeF_3 Single Crystals Doped With Sr^{2+}	IEEE. Nucl. Trans. Sci.	55(3)	1138-1141	2008
A. Yoshikawa, K. J. Kim, K. Aoki, K. Kamada, F. Saito, J. Pejchal, N. Solovieva and M. Nikl	Single Crystal Growth and Luminescence Properties of CeF_3-CaF_2 Solid Solution Grown by the Micro-Pulling-Down Method	IEEE. Nucl. Trans. Sci.	55(3)	1484-1487	2008
M. Nikl, E. Mihokova, J. Pejchal, A. Vedda, M. Fasoli, I. Fontana, V. V. Laguta, V. Babin, K. Nejezchleb, A. Yoshikawa, H. Ogino and G. Ren	Scintillator Materials-Achievements, Opportunities, and Puzzles	IEEE. Nucl. Trans. Sci.	55(3)	1035-1041	2008
M. Cadatal, Y. Furukawa, Y.-S. Seo, S. Ono, E. Estacio, H. Murakami, Y. Fujimoto, N. Sarukura, M. Nakatsuka, K. Fukuda, R. Simura, T. Suyama, A. Yoshikawa and F. Saito	Vacuum ultraviolet optical properties of a micro-pulling-down-method grown Nd^{3+}:$(La_{0.9},Ba_{0.1})F_{2.9}$	J. Opt. Soc. Am. B	25(7)	B27	2008
吉川彰、柳田健之、横田有為、荻野拓	新規シンチレータ結晶の開発と放射線検出器としての結実;発光メカニズムの選択から受光素子の選択、アレイ化、アセンブリおよび2次元マップの撮像まで	日本結晶成長学会誌	35(2)	17-23	2008
T. Yanagida, K. J. Kim, K. Kamada, K. Aoki, N. Kawaguchi, K. Fukuda and A. Yoshikawa	Measurement of Light Yield of Ce^{3+} Perturbed Emission of CaF_2 Scintillator coupled with Avalanche Photodiode	IEEE NSS/MIC 2008, N2-357 Conference Record		1162-1165	2008
柳田健之, 河口範明, 横田有為, 石津澄人, 福田健太郎, 藤本裕, 阿部直人, 吉川彰	Ce^{3+} および Pr^{3+} 添加 $YLiF_4$、$BaLiF_3$、$LiCaAlF_6$ 結晶の放射線励起時における発光特性評価	第19回光物性研究会論文集		286-289	2008

Excitation Energy Transfer in CeF_3 Single Crystals Doped With Sr^{2+}

A. Yoshikawa, K. Aoki, K. Kamada, F. Saito, M. Itoh, T. Katagiri, D. Iri, and M. Fujita

***Abstract*—CeF_3 single crystals heavily doped with Sr^{2+} ions are grown by the micro-pulling-down (μ-PD) method. The deviation of the composition in as-grown crystals is found to be entirely negligible. Three dimensional emission-excitation spectra are measured in a wide temperature range of 5–300 K by using synchrotron radiation as an exciting light source. Two intense emission bands are observed at around 320 and 400 nm. The origin of these bands is discussed on the basis of the perturbation effects introduced by Sr doping. It is pointed out that the energy transfer takes place from Ce^{3+} sites to defect sites when the crystal is warmed from 5 to 300 K.**

***Index Terms*—Crystal growth, energy conversion, fluorine compounds, luminescence, rare earth metals.**

I. Introduction

LUMINESCENCE characteristics of the Ce^{3+} centers in fluoride host crystals have been studied in a number of compounds; in particular, the 5d excited level positioning and arrangement are systematically analyzed, see [1], [2] and references therein. The Ce^{3+} emission center in fluoride hosts is of great interest for practical applications due to its high quantum efficiency at room temperature and broad emission spectrum in the ultraviolet (UV) region, which make it quite suitable for development of tunable and short-pulsed solid state lasers in this spectral region [3]–[5]. Furthermore, fast scintillation materials have been searched within Ce-doped fluorides as well. In binary fluoride compounds such as GdF_3, LaF_3, LuF_3 or CeF_3, the lowest 4f-5d absorption transition of Ce^{3+} is positioned around 250–260 nm and the related emission peaks at around 290–310 nm. However, in some cases, there is an efficient creation of so called "perturbed Ce" centers that are associated with the emission bands shifted towards 340–350 nm under the photo-excitation around 270–280 nm [6], [7]. The oxygen contamination [6] or more probably the fluorine vacancy [7]–[9] is considered as the perturber. These perturbation phenomena are described in several papers [6], [10]–[12], because the fluoride compounds doped with rare-earth ions appear favorable in the research of phosphors in light emitting devices.

In the present paper, excitation energy transfer in CeF_3 crystals doped with Sr^{2+} ions is studied through the measurements of emission-excitation spectra and luminescence decay kinetics in a wide temperature range of 5–300 K.

Manuscript received June 28, 2007; revised April 8, 2008. This work was supported in part by the Ministry of Education, Culture, Sports, Science, and Technology of Japan, Grant-in-Aid for Young Scientists (A), 19686001, 2007, and was carried out under the Joint Studies Program of the Institute for Molecular Science, Okazaki, Japan.

A. Yoshikawa, K. Kamada, and F. Saito are with the Institute of Multidisciplinary Research for Advanced Materials, Tohoku University, Sendai 980-8577, Japan (e-mail: yosikawa@tagen.tohoku.ac.jp).

K. Aoki is with the Stella Chemifa Corporation, Izumiootsu, Osaka 595-0075, Japan.

M. Itoh, T. Katagiri, and D. Iri are with the Department of Electrical and Electronic Engineering, Shinshu University, Nagano 380-8553, Japan.

M. Fujita is with the Japan Coast Guard Academy, Kure 737-8512, Japan.

Color versions of one or more of the figures in this paper are available online at http://ieeexplore.ieee.org.

Digital Object Identifier 10.1109/TNS.2008.924092

II. Experiment

A. Crystal Growth Procedure

CeF_3 single crystals heavily doped with Sr^{2+} ions (3 mol%) were grown by the micro-pulling-down (μ-PD) method [13]. Starting materials were prepared from the stoichiometric mixture of 99.99% pure CeF_3 and SrF_2 powders produced by Stella Chemifa Corporation. They were thoroughly mixed and put into a graphite crucible.

The chamber was evacuated up to 10^{-4} Torr. Then, the crucible was heated up to 600°C and kept for about 1 h at this temperature in order to remove oxygen traces caused by moisture of raw materials and adsorbates on the chamber surface. During this baking procedure, the chamber was further evacuated down to 10^{-5} Torr. After the baking, the recipient was filled with high purity Ar gas (99.999%) until ambient pressure. The crucible was heated up to about 1430°C above the melting temperature of CaF_3.

Platinum wire was used for seeding during the initial crystal growth. Further crystal growth attempts were carried out using the seed of CeF_3 crystal obtained in the initial experiments. The growth rate was 0.05–0.5 mm/min.

B. Phase Characterization

Parts of grown crystals were crashed and ground into powders. Powder X-ray diffraction analysis was carried out in the 2 θ range of 20° – 80° using a RINT Ultima (RIGAKU) diffractometer. The X-ray source was Cu $K\alpha$ (accelerating voltage: 40 kV; beam current: 40 mA).

Quantitative analyses of the crystals for Ce and Sr along the growth direction were performed by the electron probe microanalysis (EPMA) using a JXA-8621MX (JEOL). ZAF correction was made, where Z stands for the atomic number, A the absorption correction factor, and F the fluorescence correction factor.

C. Spectral Characterization

The luminescence measurements were performed by using synchrotron radiation (SR) at the beam line 1B of UVSOR in the Institute for Molecular Science, Okazaki, as a light source.

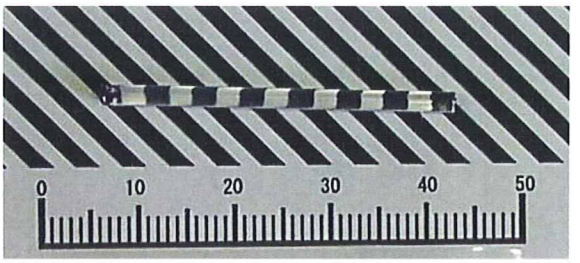

Fig. 1. Photograph of an as-grown Sr3%:CeF_3 single crystal.

The SR light was monochromatized with a 1-m Seya-Namioka type VUV monochromator. The specimens were mounted on the copper holder in a cryostat of He-flow type, allowing a wide temperature variation of 5–300 K.

Three dimensional (3-D) emission ($\lambda_{\rm em}$)-excitation ($\lambda_{\rm ex}$) spectra were measured using a SpectraPro-300i monochromator equipped with an LN/CCD camera (Roper Scientific 100EB-GI). A typical spectral resolution of the detection system was about 5 nm. The emission spectra were not corrected for the spectral response of the detection system, while the excitation spectra were corrected for the intensity distribution of the incident light. The decay kinetics of luminescence was detected by a micro-channel-plate photomultiplier (Hamamatsu R3809U-52) with use of a time-correlated single-photon counting technique when the UVSOR storage ring was operating in single-bunch mode (pulse width: 1.3 ns; pulse interval: 177.6 ns).

III. Results

A. Crystal Growth

The grown crystals were transparent and colorless. They were 2 mm in diameter and 30 mm in length. Neither visible inclusions nor cracks were observed as shown in Fig. 1.

The phase was confirmed as tysonite-type structure from the powder X-ray diffraction. No impurity phase was detected.

The deviation of the composition in the as-grown crystal was observed by EPMA and was found to be entirely negligible. Homogeneous distribution of Sr^{2+} and Ce^{3+} in $(Sr_xCe_{1-x})F_{3-x}$ single crystal could be observed as shown in Fig. 2.

B. Luminescence Characteristics

Fig. 3 shows the 3-D emission-excitation spectrum of Sr3%:CeF_3 crystals at 6 K, together with the contour plot of the 3-D spectrum in the ($\lambda_{\rm em}$, $\lambda_{\rm ex}$) plane. An emission band peaking at 320 nm is excited with UV light at $\lambda_{\rm ex} < 290$ nm. This band somewhat red-shifts relative to the Ce^{3+} 5d $\rightarrow$ 4f luminescence (287 and 304 nm) in pure CeF_3 [8]. The excitation threshold (290 nm) is also lowered as compared to that (260 nm) for the intrinsic Ce^{3+} luminescence. The doublet luminescence peaking around 287 and 304 nm were observed in our undoped CeF_3 sample, as well. Therefore, the 320 nm luminescence in Sr:CeF_3 system is understood as low-energy shifted band of the intrinsic luminescence from Ce^{3+}. These facts suggest that the 320 nm band is ascribed to Ce^{3+} ions perturbed weakly by Sr^{2+} ions. The intrinsic Ce^{3+} luminescence locating on the short-wavelength side of the main band at 320 nm is very weak in intensity due to heavy doping and is observable as a shoulder-like structure.

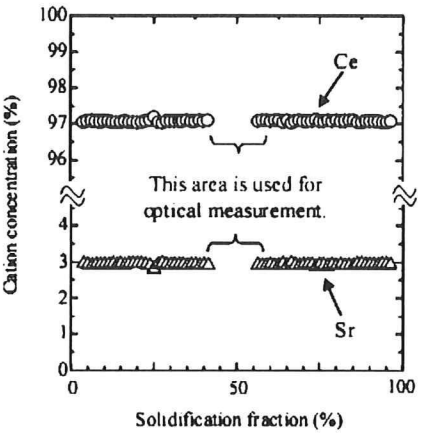

Fig. 2. Cation distribution in $(Sr_xCe_{1-x})F_{3-x}$ single crystal. ○ and △ indicate Ce and Sr, respectively.

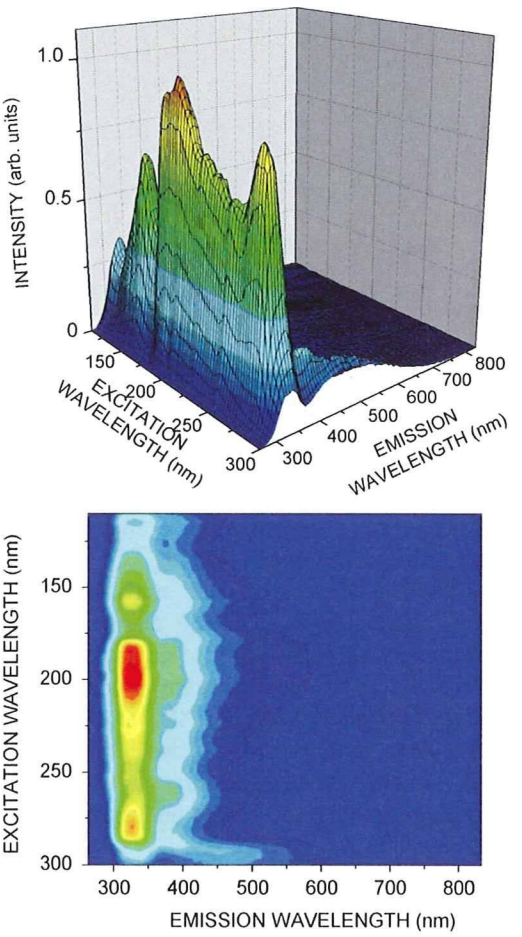

Fig. 3. 3-D emission-excitation spectrum of Sr3%:CeF_3 crystal at 6 K, together with the contour plot of the upper spectrum in the ($\lambda_{\rm em}$, $\lambda_{\rm ex}$) plane.

Fig. 4 shows the 3-D emission-excitation spectrum measured at 300 K, together with the contour plot of the 3-D spectrum in the ($\lambda_{\rm em}$, $\lambda_{\rm ex}$) plane. In this fugure, a broad emission band appears at around 400 nm at the expense of the 320 nm band. The 400 nm band is excited at $\lambda_{\rm ex} < 295$ nm. This band is

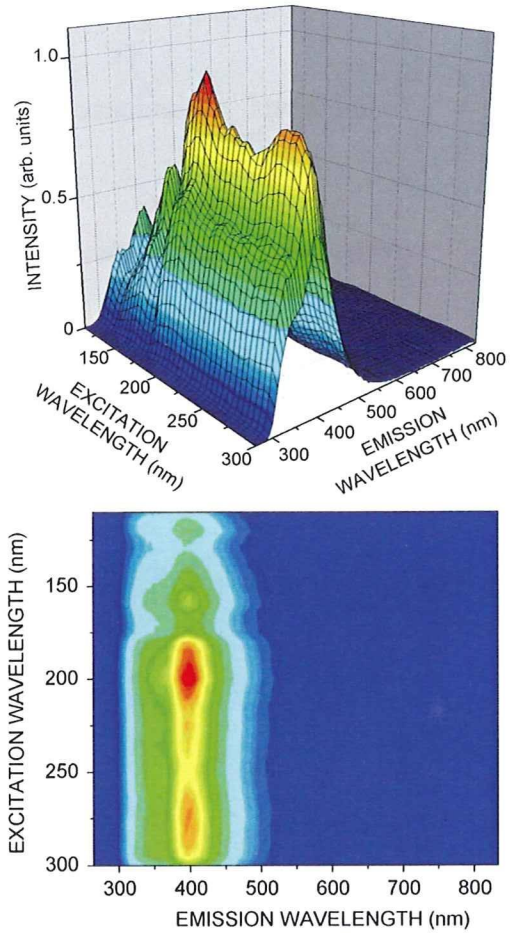

Fig. 4. 3-D emission-excitation spectrum of Sr3%:CeF_3 crystal at 300 K, together with the contour plot of the upper spectrum in the $(\lambda_{em}, \lambda_{ex})$ plane.

probably attributed to some lattice defect that was introduced by Sr^{2+} doping, as will be discussed later.

Temperature dependence of the emission spectra of Sr3%:CeF_3 is shown in Fig. 5. The excitation was made at $\lambda_{ex} = 140$ nm, which corresponds to the intrinsic absorption region of CeF_3 [14]. As the temperature is increased, the 320 nm band is getting lower, while the 400 nm band is getting higher. The relative peak intensity of both bands is reversed around 240 K. A weak broadband is observed at around 540 nm at 5 K and disappears with increasing temperature. The origin of this band is not clear at present.

Fig. 6 shows the decay behaviors of (a) the 320 nm luminescence at 6 K and (b) the 400 nm luminescence at 300 K. The excitation was made at $\lambda_{ex} = 266$ nm, which corresponds to the spectral region of pertutbed Ce^{3+} 4f→5d absorption bands [14]. The two emision bands exhibit a single exponetial decay over two decades. The decay times of the 320 and 400 nm bands are 26 and 40 ns, respectively. These values are comparable with the decay time (17 ns at 6 K, see Fig. 7) of the intrinsic Ce^{3+} luminescence. This fact suggests a possibility that these two bands are related to some kind of Ce^{3+} luminescent centers.

IV. Discussion

When Sr^{2+} ions substitute Ce^{3+} sites, the introduction of at leaset two candidates for perturber is expected;

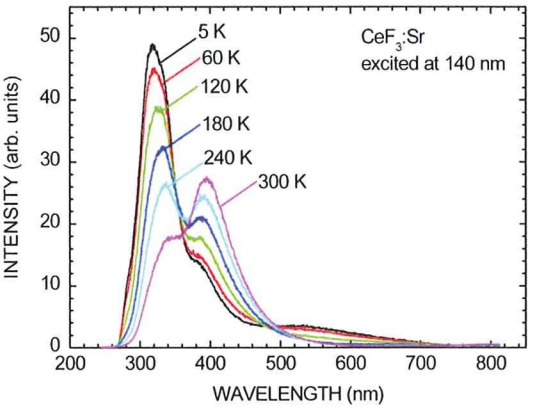

Fig. 5. Temperature dependence of the emission spectra of Sr3%:CeF_3 crystal exited at $\lambda_{ex} = 140$ nm.

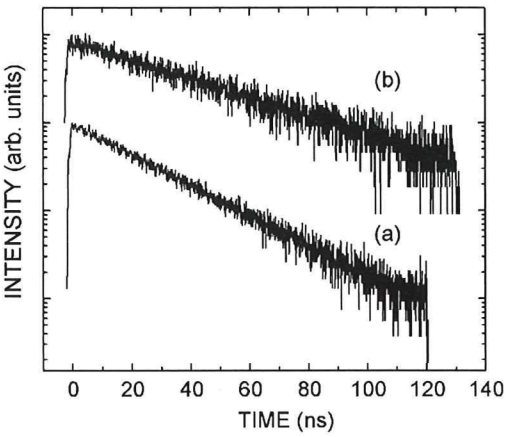

Fig. 6. Decay curves of (a) the 320 nm luminescence at 6 K and (b) the 400 nm luminescence at 300 K, under the excitation at $\lambda_{ex} = 266$ nm.

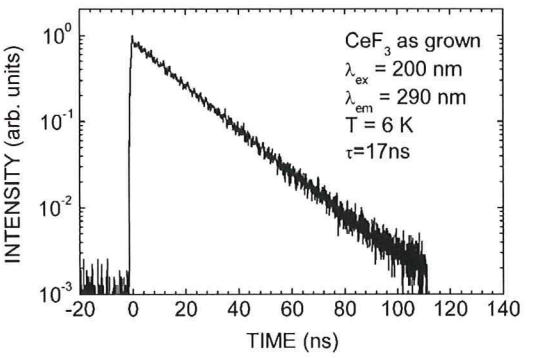

Fig. 7. Decay time of the intrinsic Ce^{3+} luminescence of undoped CeF_3 at 6 K.

1() Ce^{3+} luminescent center is perturbed by the neighboring Sr^{2+} ion itself.

2() F^- vacancy is generated depending on the amount of substitution. As a result, Ce^{3+} luminescent state is modified by the nearby F^- vacancy.

In the case of (1), the influence of a perturber is supposed to be relatively small. This likely corresponds to the 320 nm luminescence band, because the red-shift from the intrinsic Ce^{3+}

luminescence is only 6–23 nm. In the case of (2), the perturbation effect might be greater than that of (1), because the F^- vacancy could largely deform the surrounding lattice. Most probably, a complex center consisting of Ce^{3+} and F^- vacancy will be produced, from which the 400 nm luminescence is emitted. Of course, there may be a possibility that the 400 nm luminescence originates from the radiative recombination of an electron with a hole at the sites without Ce^{3+} ions.

From Fig. 5, one may understand that the 400 nm band is enhanced in intensity at the expense of the 320 nm band when the Sr3%:CeF_3 crystal is warmed from 5 to 300 K. Therefore, it is supposed that excitation energy is efficiently transferred from Ce^{3+} sites to defect sites under the excitaion of the host crystal at room temperature.

V. Conclusion

The CeF_3 single crystals heavily doped with Sr^{2+} ions were grown by the micro-pulling-down (μ-PD) method. It was confirmed that the deviation of the composition in as-grown crystals is entirely negligible. The luminescence spectra and decay kinetics were investigated in a wide temperature range between 5 and 300 K. Two emission bands were observed at 320 and 400 nm. We supposed that the former arises from the Ce^{3+} ions perturbed by neighboring Sr^{2+} ions and the latter probably from the complex center consisting of Ce^{3+} and F^- vacancy. It was pointed out that the energy transfer from Ce^{3+} sites to defect sites takes place efficiently at room temperature. Further studies are desired for understanding of the mechanism of the energy transfer in Sr3%:CeF_3 crystal, along with the origin of the 540 nm luminescence band observed at low temperatures.

References

[1] N. Kodama, M. Yamaga, and B. Henderson, "Energy levels and symmetry of Ce^{3+} in fluoride and oxide crystals," *J. Appl. Phys.*, vol. 84, pp. 5820–5822, 1998.

[2] P. Dorenbos, "5 *d* -level energies of Ce^{3+} and the crystalline environment. I. Fluoride compounds," *Phys. Rev. B*, vol. 62, pp. 15640–15649, 2000.

[3] D. J. Ehrlich, P. F. Moulton, and R. M. Osgood, "Optically pumped Ce:LaF_3 laser at 286 nm," *Opt. Lett.*, vol. 5, p. 39, 1980.

[4] C. D. Marshall, J. A. Speth, S. A. Payne, W. F. Krupke, G. J. Quarles, V. Castillo, and B. H. T. Chai, "Ultraviolet laser emission properties of Ce^{3+} -doped $LiSrAlF_6$ and $LiCaAlF_6$," *J. Opt. Soc. Amer. B*, vol. 11, p. 2054, 1994.

[5] Z. Liu, K. Shimamura, K. Nakano, T. Fukuda, T. Kozek, H. Ohtake, and N. Sarukura, "High-pulse-energy ultraviolet Ce^{3+} :$LiCaAlF_6$ laser oscillator with newly designed pumping schemes," *Jpn. J.Appl. Phys.*, vol. 39, pp. L466–467, 2000.

[6] G. Blasse, "Energy Transfer Phenomena in the System (Y, Ce, Gd, Tb) F_3," *Phys. Status Solidi (a)*, vol. 73, pp. 205–208, 1982.

[7] C. Pedrini, B. Moine, J. C. Gacon, and B. Jacquier, "One- and two-photon spectroscopy of Ce^{3+} ions in LaF_3 -CeF_3 mixed crystals," *J. Phys. Cond. Matter.*, vol. 4, pp. 5461–5470, 1992.

[8] A. J. Wojtowicz, M. Balcerzyk, E. Berman, and A. Lempicki, "Optical spectroscopy and scintillation mechanisms of $Ce_x La_{1-x} F_3$," *Phys. Rev. B*, vol. 49, pp. 14880–14895, 1994.

[9] M. Nikl and C. Pedrini, "Photoluminescence of heavily doped CeF_3 : Cd^{2+} single crystals," *Solid State Commun.*, vol. 90, pp. 155–159, 1994.

[10] M. J. J. Lammers and G. Blasse, "Luminescence properties of rare-earth-activated gadolinium fluoride (GdF_3) and oxyfluorides (GdOF)," *Phys. Status Solidi (b)*, vol. 127, pp. 663–671, 1985.

[11] S. H. M. Poort, A. Meyerink, and G. Blasse, "On the luminescence of GdF_3 : Ce^{3+}, Mn^{2+}," *Solid State Commun.*, vol. 103, pp. 537–540, 1997.

[12] Nikl, "Wide band gap scintillation materials: progress in the technology and material understanding," *Phys. Status Solidi (a)*, vol. 178, p. 95, 2000.

[13] A. Yoshikawa, T. Satonaga, K. Kamada, H. Sato, M. Nikl, N. Solovieva, and T. Fukuda, "Crystal growth of Ce: PrF_3 by micro-pulling-down method," *J. Cryst. Growth*, vol. 270, pp. 427–432, 2004.

[14] C. G. Olson, M. Piacentini, and D. W. Lynch, "Optical properties of single crystals of some rare-earth trifluorides, 5–34 eV," *Phys. Rev. B*, vol. 18, p. 740, 1978.

Single Crystal Growth and Luminescence Properties of CeF_3-CaF_2 Solid Solution Grown by the Micro-Pulling-Down Method

Akira Yoshikawa, Kyoung Jin Kim, Kenji Aoki, Kei Kamada, Fumio Saito, Jan Pejchal, Natalia Solovieva, and Martin Nikl

***Abstract*—$(Ce_xCa_{1-x})F_{2+x}$ single crystal with x = 0.0001 – 0.03 were grown by the μ-PD method. Ce^{3+} doping in CaF_2 lattice gives rise to characteristic absorption and emission bands, which are governed by the characteristics of the isolated Ce^{3+}-F_i^- C_{4v} pair centers and small clusters composed from these pairs. With increasing Ce concentration there is a strong increase of the absorption bands related to the cluster centres, but the radioluminescence spectra are always governed by the emission of the isolated Ce^{3+}-F_i^- C_{4v} pairs without noticeable changes in the emission band shape. Highest radioluminescence intensity is achieved for Ce0.1{%} concentration and above 1{%} of Ce the onset of concentration quenching is observed. Scintillation response is governed by the energy transfer from the CaF_2 host lattice and even for the Ce3{%} sample the dominant scintillation decay time is about 50{%} longer with respect to the photoluminescence decay time of Ce^{3+}-F_i^- C_{4v} pair centres. Energy transfer processes and the role of different Ce^{3+}-based centers are discussed.**

***Index Terms*—Ce perturbed center, crystals, fluoride, scintillator.**

I. Introduction

LUMINESCENCE characteristics of the Ce^{3+} doped CaF_2 were reported already in the sixties [1], [2]. As Ce^{3+} ion resides at the Ca^{2+} site there is a need for a charge compensation, which is accomplished by an interstitial F^- ion at the vacant cationic sites of the cubic CaF_2 lattice. Depending on the position of F^-, the Ce^{3+} centers with tetragonal C_{4v} (nn position of F^-) or trigonal C_{3v} (nnn position of F^-) symmetry are created [3]. The former center is dominating and its absorption bands are found at about 307 nm (4f-5d(e_g)) and 190–210 nm (4f-5d(t_{2g})), while its luminescence occurs in typical Ce^{3+} double peak spectrum at 318 nm and 339 nm with a decay time around 40 ns [4].When Ce^{3+} concentration is higher than approximately 0.005% the aggregation of Ce^{3+}-F_i^- pairs starts and rhombic symmetry cluster centres consisting of two or four such pairs appear [5], for which the absorption bands around 245 nm and 215 nm are typical. Under excitation at 245 nm the leading luminescence peak occurs at 290–310 nm accompanied by a shoulder within 360–400 nm with the decay times of about 28 ns and 48 ns, respectively [4].

Despite of low density the CaF_2 host has been exploited for scintillator materials. At RT the CaF_2 itself shows bright self-trapped emission luminescence at about 280 nm. The doping with Eu^{2+} provided scintillator with very high light yield, but of rather slow response of about 900 ns due to 5d1-4f radiative transition of Eu^{2+} center [6].

It is the aim of this paper to report the absorption, photoluminescence and scintillation characteristics of CaF_2:Ce in a broad concentration range (0.01–3% of Ce). Energy transfer processes and the role of different Ce^{3+}-based centers mentioned above are discussed.

II. Experimental Procedure

A. Crystal Growth Procedure

Single crystals of solid solution between CeF_3 and CaF_2 were grown by the micro-pulling-down (μ-PD) method, the description of which can be found in [7], [8]. Starting materials were prepared from the stoichiometric mixture of 99.99% pure CeF_3 and CaF_2 powders produced by Stella Chemifa Corporation. They were thoroughly mixed and put into a graphite crucible.

The chamber was evacuated up to 10^{-4} Torr. Then, the crucible was heated up to 600°C and kept for about 1 hour at this temperature in order to remove oxygen traces caused by moisture of raw materials and adsorbates on the chamber surface. During this baking procedure, the chamber was further evacuated down to 10^{-5} Torr. After the baking, the recipient was filled with high purity Ar gas (99.999%) and CF_4 gas (99.999%) until ambient pressure. The crucible was heated up to about 1400°C above the melting temperature of CaF_2.

CaF_2 single crystal grown by Cz method was used for the seed. The growth rate was 0.02–0.5 mm/min.

B. Phase Characterization

Parts of grown crystals were crashed and ground into powders. Powder X-ray diffraction analysis was carried out in the 2θ range of $20° - 80°$ using a RINT Ultima (RIGAKU) diffractometer. The X-ray source was CuKα (accelerating voltage: 40 kV; beam current: 40 mA).

Manuscript received June 28, 2007; revised April 8, 2008. This work was supported in part by the Ministry of Education, Culture, Sports, Science, and Technology of Japan, Grant-in-Aid for Young Scientists (A), 19686001, 2007, JSPS-ASCR Joint Research Project and Czech MSMT KONTAKT ME953 project.

A. Yoshikawa, K. J. Kim, K. Kamada, and F. Saito are with the Institute of Multidisciplinary Research for Advanced Materials, Tohoku University, Sendai 980-8577, Japan (e-mail: yosikawa@tagen.tohoku.ac.jp).

K. Aoki is with the Stella Chemifa Corporation, Izumiootsu, Osaka 595-0075, Japan.

J. Pejchal, N. Solovieva, and M. Nikl are with the Institute of Physics AS CR, 16253 Prague, Czech Republic.

Color versions of one or more of the figures in this paper are available online at http://ieeexplore.ieee.org.

Digital Object Identifier 10.1109/TNS.2008.924091

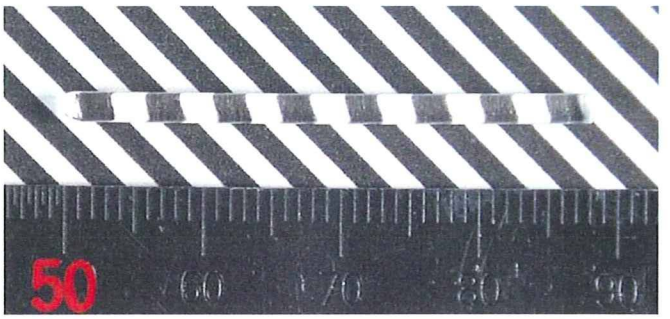

Fig. 1. Photograph of an as-grown Ce3%:CaF_2 single crystal.

Quantitative analyses of the crystals for Ce and Ca along the growth direction were performed by the electron probe microanalysis (EPMA) using a JXA-8621MX (JEOL). ZAF correction was made, where Z stands for the atomic number, A the absorption correction factor, and F the fluorescence correction factor.

C. Optical Characterization

Absorption spectra were measured by UV—VIS—NIR spectrophotometer Shimadzu UV-3101PC. Luminescence measurements were performed by the Spectrofluorometer 199S (Edinburgh Instruments) equipped with the hydrogen steady-state lamp and x-ray tube for excitation. Time-correlated single photon counting method was employed to measure scintillation decay under 511 keV photon excitation from ^{22}Na radioisotope. All measurements are performed at room temperature (RT). Luminescence spectra were corrected for experimental distortions. Exponential approximation of the decays was obtained by performing the convolution of the considered function with the instrumental response and the least-square sum fitting procedure (Software package Spectrasolve from LASTEK Ltd.)

III. Result and Discussion

A. Crystal Growth

The grown crystals were transparent and colorless. They were 2 mm in diameter and 30 mm in length. Neither visible inclusions nor cracks were observed as shown in Fig. 1.

The phase of the fluorite-type structure with space group of Fm-3 m was confirmed from the powder X-ray diffraction. No impurity phase was detected.

The deviation of the composition in the as-grown crystal was measured by EPMA and very homogeneous distribution of Ce^{3+} in $(Ce_xCa_{1-x})F_{2+x}$ single crystal was found. As an example, the cation distribution of Ce3%: CaF_2 is shown in Fig. 2. (All the dopant concentration in this manuscript is described in atomic %.)

B. Optical Characterization

In Fig. 3 the absorption spectra of selected crystals from the concentration set are given. The absorption bands related to Ce^{3+}-F_i^- C_{4v} pairs and rhombic symmetry clusters are noted.

Apparently, the dependence of the 306 nm and 190–210 nm peaks on the Ce concentration is sublinear, while steeper (even

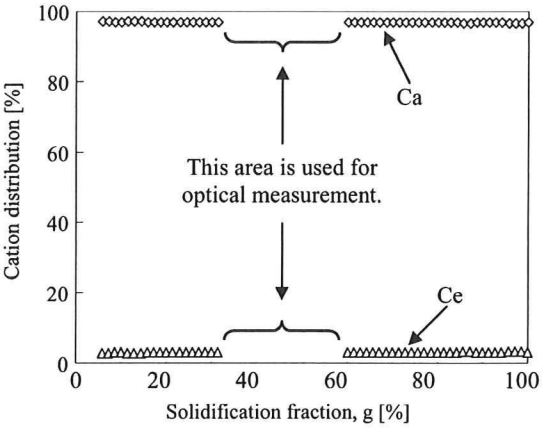

Fig. 2. Cation distribution in Ce3%: CaF_2 single crystal.

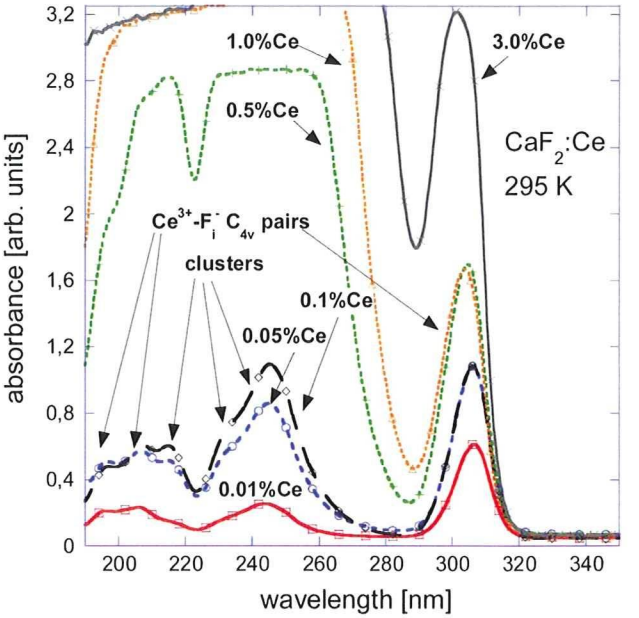

Fig. 3. Absorption spectra of Ce: CaF_2 sample set at RT.

if still possibly sublinear) dependence holds for the peaks within 215–280 nm, which is explained by the composition of related Ce-based centres. It is interesting to note slight high energy shift of the 306 nm peak with increasing Ce concentration, which might be due to gradual splitting of the e_g level of Ce^{3+}-F_i^- centers possibly due to an external perturbation. It may arise e.g., due to vicinity of other Ce-based centres. Small splitting of the e_g level is most probably due to C_{4v} tetragonal site symmetry which can be still considered like a small departure from cubic symmetry in which the e_g level remains unsplitted yet, see [9] for an overview of Ce^{3+} absorption bands-versus-symmetry considerations in various fluorides.

In Fig. 4 the photoluminescence spectra measured at the lowest Ce concentration sample are given. The peak of excitation spectrum related to the emission of Ce^{3+}-F_i^- C_{4v} centers is well correlated with the absorption spectrum in Fig. 1, but there is no immediate explanation for a shoulder around 280 nm, where the absorption of the sample is rather low. Emission spectrum is measured under excitation into the cluster centres.

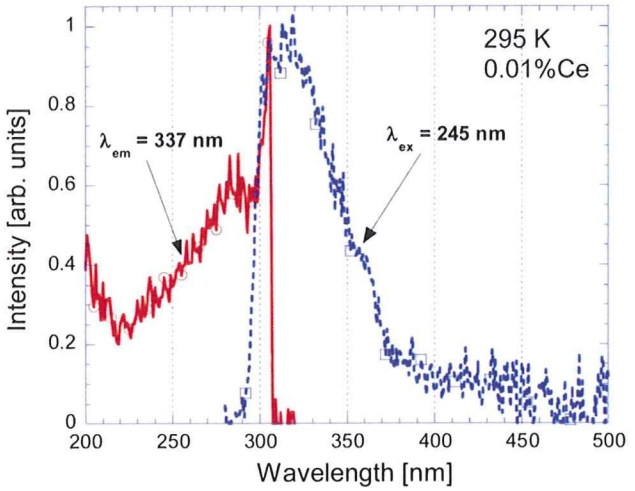

Fig. 4. Excitation ($\lambda_{em} = 337$ nm) and emission ($\lambda_{ex} = 245$ nm) spectra at RT of Ce0.01%:CaF_2. Due to the measurement geometry (90 degrees) the intensity at the high energy side of the emission spectrum might be lowered due to sample reabsorption.

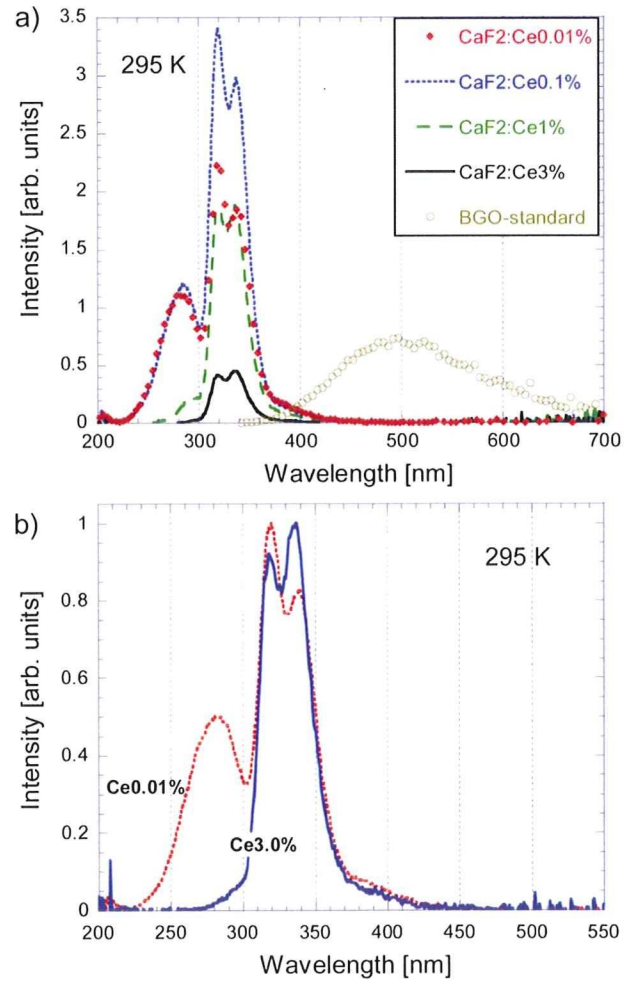

Fig. 5. (a) Absolute radioluminescence spectra (X-ray tube, 25 kV) of the CaF_2:Ce sample set in comparison with the BGO standard sample. (b) Normalized radioluminescence spectra for the limit Ce concentrations.

It is high-energy shifted with respect to that of Ce^{3+}-F_i^- C_{4v} centers in agreement with the literature [4] (see also Fig. 5) and shows the longer wavelength tail towards 400 nm as well.

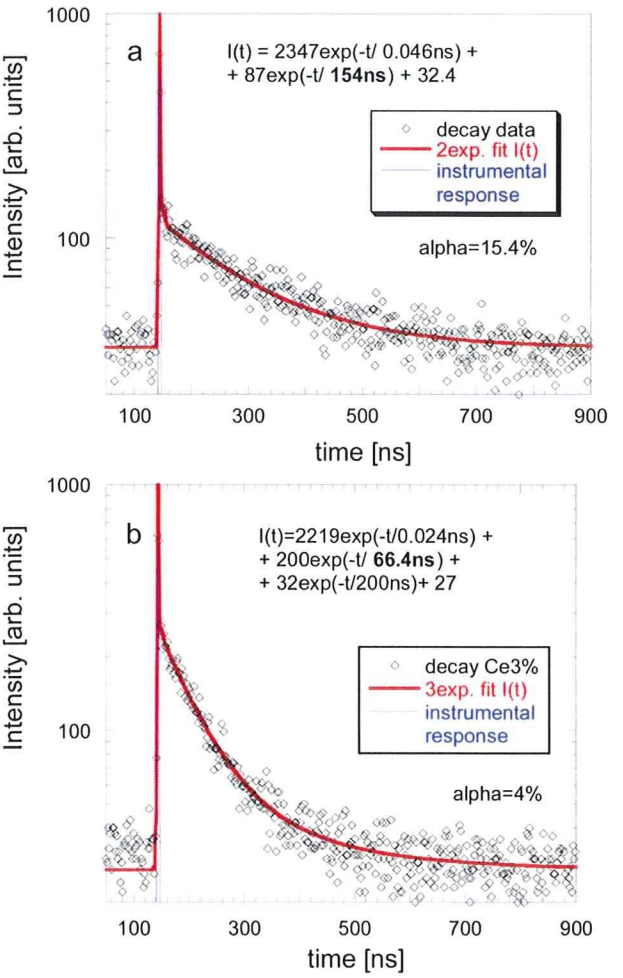

Fig. 6. Spectrally unresolved scintillation decays of Ce: CaF_2 under excitation of 511 keV photons from ^{22}Na radioisotope. (a) Ce1%:CaF_2; (b) Ce3%:CaF_2. Solid line is the convolution of the instrumental response (also in the figure) and function I(t). The subnanosecond component is due to an instrumental effect and has no physical meaning.

In radioluminescence spectra in Fig. 5 the Ce^{3+}-F_i^- C_{4v} centers are dominating. The self-trapped exciton emission band at 280 nm is gradually suppressed with increasing Ce concentration, but becomes completely dumped only for the highest Ce3% sample. The highest emission intensity is achieved for Ce0.1% sample and rapid intensity decrease is observed for the Ce3% one. The latter phenomenon can be probably explained by the concentration quenching onset between 1–3% of Ce concentration in CaF_2 host. It is interesting to note that despite of enormously increasing concentration of cluster centers (see Fig. 3), their contribution at the long-wavelength side of the spectrum is relatively constant and very low (Fig. 5(b)). As noted in [4] there is an energy transfer from the cluster-based emission within 290–310 nm to the isolated Ce^{3+}-F_i^- C_{4v} centers, which explains the absence of this band in RL spectrum, but the same explanation can be hardly adopted for the lower energy lying emission at 360–400 nm unless there would be a common parent state for both the 290–310 nm and 360–400 nm emissions in the cluster centres.

Scintillation decays of Ce1% and Ce3% samples are given in Fig. 6(a), (b), respectively. Noticeable shortening of the domi-

nant decay time from 154 ns to 66 ns is obtained increasing the Ce concentration from 1% to 3%. However, even in the latter case the decay time is substantially longer with respect to the reported Ce^{3+}-F_i^- C_{4v} centers photoluminescence one, which is about 40 ns [4]. An energy transfer from the host lattice (most probably via the self-trapped exciton) can slow-down the scintillation response so that an intrinsic limit given by the photoluminescence decay time (40 ns) of the emission center cannot be reached. Displayed value of coefficient alpha is related to the occurrence of very slow decay components in the range of tens-hundreds of μs [10]. With increasing Ce concentration their content is clearly diminished.

IV. Conclusion

$(Ce_xCa_{1-x})F_{2+x}$ single crystal with $x = 0.0001, 0.001, 0.01$ and 0.03 were grown by the μ-PD method. They are transparent and free of visible defects. Homogeneous distribution of Ce in CaF_2 is observed in all the crystals.

Ce^{3+} doping in CaF_2 lattice gives rise to characteristic absorption and emission bands, which are governed by the characteristics of the isolated Ce^{3+}-F_i^- C_{4v} pair centers and small clusters composed from these pairs. With increasing Ce concentration there is a strong increase of the absorption bands related to the cluster centres, but the radioluminescence spectra are always governed by the emission of the isolated Ce^{3+}-F_i^- C_{4v} pairs without noticeable changes in the emission band shape. Highest radioluminescence intensity is achieved for Ce0.1% concentration and above 1% of Ce the onset of concentration quenching is observed. Scintillation response is governed by the energy transfer from the CaF_2 host lattice and even for the Ce3% sample the dominant scintillation decay time is about 50% longer with respect to the photoluminescence decay time of Ce^{3+}-F_i^- C_{4v} pair centres.

References

[1] M. J. Weber and R. W. Bierig, "Paramagnetic resonance and relaxation of trivalentt rare-earth ions in calcium fluoride. I. Resonance spectra and crystal fields.fields," *Phys. Rev. 134*, vol. A1492, 1964.

[2] J. M. Baker, E. R. Davies, and J. P. Hurrell, *Phys. Lett. A 26*, vol. 352, 1968.

[3] W. J. Manthey, *Phys. Rev. B 8*, vol. 4086, 1973.

[4] S. B. Mirov, A. Y. Dergachev, W. A. Sibley, V. B. Sigachev, A. G. Papalashvili, and T. T. Basiev, "Investigation of luminescence properties of Ce:Sc:CaF_2 crystals," *Mater. Sci. Forum*, vol. 239–241, pp. 227–230, 1997.

[5] V. V. Osiko, Y. K. Voronko, and A. A. Sobol, *In Crystals 10: Growth, Properties and Applications*, H. C. Freyherdt, Ed. Berlin, Germany: Springer-Verlag, 1984, pp. 37–86.

[6] J. Menefee, C. F. Swinehart, and E. W. O'Dell, *IEEE Trans. Nucl. Sci.*, vol. 720, 1966.

[7] A. Yoshikawa, T. Satonaga, K. Kamada, H. Sato, M. Nikl, N. Solovieva, and T. Fukuda, "Crystal growth of Ce: PrF_3 by micro-pulling-down method," *J. Cryst. Growth*, vol. 270, pp. 427–432, 2004.

[8] A. Yoshikawa, M. Nikl, G. Boulon, and T. Fukuda, "Challenge and study for developing of novel single crystalline optical materials using micro-pulling-down method," *Opt. Mater.*, vol. 30, pp. 6–10, 2007.

[9] P. Dorenbos, "5d-level energies of Ce^{3+} and the crystalline environment. I. Fluoride compounds," *Phys. Rev. B*, vol. 62, pp. 15640–15649, 2000.

[10] M. Nikl, K. Nitsch, K. Polak, E. Mihokova, I. Dafinei, E. Auffray, P. Lecoq, P. Reiche, and R. Uecker, "Slow components in the photoluminescence and scintillation decays of $PbWO_4$ single crystals," *Phys. Status Solidi (b)*, vol. 195, pp. 311–323, Jan. 1996.

Scintillator Materials—Achievements, Opportunities, and Puzzles

M. Nikl, E. Mihokova, J. Pejchal, A. Vedda, M. Fasoli, I. Fontana, V. V. Laguta, V. Babin, K. Nejezchleb, A. Yoshikawa, H. Ogino, and G. Ren

***Abstract*—Participation of shallow and deep traps in the processes of energy transfer and capture is studied by means of time-resolved emission spectroscopy and thermoluminescence in several groups of the Ce^{3+} and Pr^{3+}-doped complex oxide single crystal scintillators. Tunnelling-driven recombination processes are distinguished in all the groups of examined materials: closely spaced electron and hole traps give rise to the t^{-1} phosphorescence decays at low temperatures in the Ce-doped aluminum garnets and perovskites, while thermally assisted tunneling process is proposed to explain temperature independent trap depth in glow curve peaks within 50–250° C in Ce-doped lutetium orthosilicates.**

***Index Terms*—LuAG:Ce, LuAG:Pr, LuYAP:Ce and LYSO:Ce single crystals, points defects and traps, scintillators.**

I. Introduction

DESPITE the relatively long history of the development of scintillator and phosphor materials started at the end of 19th century, within the last two decades the scintillator characteristics and figure-of-merit of a number of new materials were studied and some of the materials were successfully industrialized. In particular, Ce-doped silicates, aluminum perovskites and garnets, trivalent-ion-doped $PbWO_4$ and Ce-doped binary rare earth halides are worth mentioning, for recent reviews see [1]–[4]. An interest in new scintillator materials is pushed by increasing number of medical, industrial or scientific applications, requiring higher material performance. To optimize materials towards their intrinsic limits, understanding of energy transfer and storage processes, specific defects and their relation to the manufacturing technology appear of crucial importance [1], [4]. Deep electron traps and their role in the afterglow of the Ce-doped silicates, shallow electron traps related to antisite defects in aluminum garnets or appearance of slower scintillation components and drop of the light yield in mixed (Y-Lu) aluminum perovskites are just a few examples of current problems in the field. These problems should be studied and appropriate technological solutions should be found to further improve the material performance.

The aim of this paper is to review the current understanding of the role of selected defects in the processes of energy transfer and carrier capture in the above mentioned materials belonging to complex oxide scintillators.

Manuscript received June 28, 2007; revised September 27, 2007. This work was supported by the Czech GACR 202/05/2471, MSMT KONTAKT ME903, ME953, GA AV S100100506 and "Italian Cariplo foundation 2006-2008 structure and optical properties of self-organized nano- and mesoscopic materials" projects and by the EC—Research Infrastructure Action under the FP6 "Structuring the European Research Area" Program (through the Integrated Infrastructure Initiative Integrating Activity on Synchrotron and Free Electron Laser Science).

M. Nikl is with the Institute of Physics AS CR, 162 53 Prague, Czech Republic and also with the Department. of Materials Science, University of Milano-Bicocca, 20125 Milan, Italy (e-mail: nikl@fzu.cz).

E. Mihokova and J. Pejchal are with the Institute of Physics AS CR, 162 53 Prague, Czech Republic (e-mail:mihokova@fzu.cz; pejchal@fzu.cz).

A. Vedda, M. Fasoli and I. Fontana are with the Department of Materials Science, University of Milano-Bicocca, 20125 Milan, Italy (e-mail: anna.vedda@mater.unimib.it; mauro.fasoli@mater.unimib.it; ilaria.fontana@mater.unimib.it).

V. V. Laguta is with the Institute of Problems in Materials Science UAS, 03142 Kiev, Ukraine and also with the Institute of Physics AS CR, 162 53 Prague, Czech Republic (e-mail: laguta@ipms.kiev.ua).

V. Babin is with the Institute of Physics, University of Tartu, 51 014 Tartu, Estonia (e-mail: vladimir.babin@ut.ee).

K. Nejezchleb is with the Crytur Ltd., 51119 Turnov, Czech Republic (e-mail: nejezchleb@crytur.cz).

A. Yoshikawa is with IMRAM, Tohoku University, 980-8577 Sendai, Japan (e-mail: yosikawa@tagen.tohoku.ac.jp).

H. Ogino is with the School of Engineering, The University of Tokyo, 113-8656 Tokyo, Japan (e-mail: tuogino@mail.ecc.u-tokyo.ac.jp).

G. Ren is with the Shanghai Institute of Ceramics (SIC), 200050 Shanghai, China (e-mail: rgh@mail.sic.ac.cn).

Color versions of one or more of the figures in this paper are available online at http://ieeexplore.ieee.org.

Digital Object Identifier 10.1109/TNS.2007.913480

II. Samples and Experimental Technique

Ce- doped single crystals of $Lu_3Al_5O_{12}$, (Y-Lu)AlO_3 and Lu_2SiO_5 were grown in some of the institutions where the coauthors belong, namely: CRYTUR (perovskites $YAlO_3$ (YAP), (Lu-Y)AlO_3 (LuYAP) and garnets $Lu_3Al_5O_{12}$ (LuAG)) or SIC (silicates Lu_2SiO_5 (LSO), Y_2SiO_5(YSO), (Lu-Y)$_2SiO_5$ (LYSO)) by Czochralski method from the high temperature melt from the raw materials with at least 4N purity. Pr-doped and Ga-admixed aluminum garnets were grown in IMRAM from the raw materials of the same purity using the micropulling-down (m-PD) and Czochralski methods. Plates up to $7 \times 7 \times 1$ mm, polished to an optical grade, were prepared for luminescence experiments.

Measurements of photoluminescence (PL) and radioluminescence (RL) spectra as well as the PL and scintillation decays, were performed with the Spectrofluorometer 199S (Edinburgh Instruments) equipped with pulsed UV flashlamps, steady-state H2-lamp and X-ray tube (35–40 kV, Mo-anticathode) and ^{22}Na radioisotope (511 keV photons) excitation sources. Emission spectra were corrected for the spectral response of the system. Convolution of the multi-exponential function with the instrumental response was used to find the correct decay-time values in the decays extended to ns time scales. TSL measurements were performed after X-irradiation at 10 K (by a Philips 2274 X-ray tube operated at 20 kV) or at RT (by a Machlett OEG50 X-ray tube operated at 30 kV). In the low-T range (10–300 K)

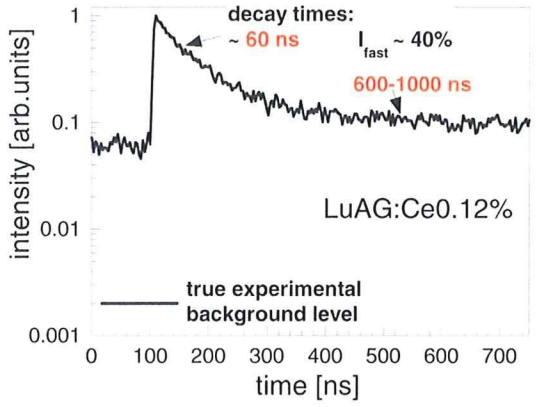

Fig. 1. Spectrally unresolved scintillation decay of the 0.12%Ce-doped sample excited at RT by 511 keV photons from ^{22}Na radioisotope.

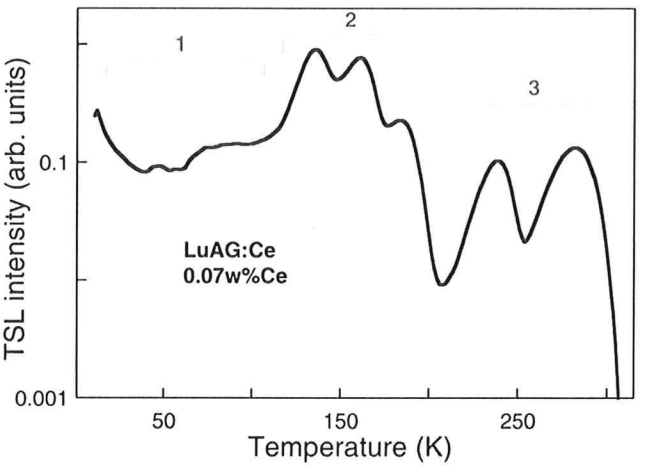

Fig. 2. TSL glow curve of LuAG:Ce after X-irradiation at 10 K.

we performed wavelength resolved measurements with a detection system using a monochromator coupled to a CCD detector (Jobin-Yvon Spectrum One 3000) operating in the 280–710 nm interval. A heating rate of 0.1 K/s was adopted. High-T measurements (from RT to 400°C) were performed with a heating rate of 1°C/s and TSL emission was detected by a photomultiplier (EMI9635QB).

III. Experimental Results and Discussion

A. Ce- and Pr-doped Aluminum Garnets

Ce^{3+}-doped $Y_3Al_5O_{12}$ (YAG) single crystal for fast scintillator applications was reported in the literature already in the seventies [5]. The first comprehensive description of YAG:Ce scintillator characteristics was reported by Moszynski *et al.* [6], who included this material in the high figure-of-merit oxide scintillators. Isostructural LuAG has a higher density (6.67 g/cm^3) than YAG (4.56 g/cm^3), which is advantageous in the case of hard X- and γ-ray detection. LuAG:Ce scintillator became of interest relatively recently [7], [8]. The m-PD grown Pr-doped LuAG scintillator was for the first time mentioned in the literature in 2005 [9] and further improved using the Czochralski technique [10]: light yield approaching 300% of $Bi_4Ge_3O_{12}$ (BGO), spectrally uncorrected, and the dominant decay time of about 20 ns include this material in the group of the fastest, high light yield and high density materials available today.

Recent studies revealed a considerable percentage of slow, technically unexploitable light in the scintillation response of aluminum garnet scintillators, especially in those LuAG-based [11]. Typical scintillation decay of LuAG:Ce is given in Fig. 1. While the dominant component has a decay time very similar to that of PL decay (54 ns), a slower decay process that can be fit by an exponential with 600–1000 ns decay time is always found.

Moreover, the signal increase before the rising edge of the decay (with respect to the true experimental background level given essentially by the detector electronic noise) points to the presence of very slow decay processes the time constant of which is comparable with the time interval between two subsequent excitation events (tens-to-hundreds of microseconds) [11]. The low temperature TSL glow curve reveals a number of trapping states and three typical regions can be distinguished (so far more than twenty different single crystals of Ce^{3+} and Pr^{3+} doped LuAG have been measured), see Fig. 2. Region 2 is related to the shallow electron trap due to an antisite Lu_{Al} defect (AD) [12], [13], responsible also for the intrinsic luminescence of undoped LuAG, see Fig. 3. ADs in isostructural YAG were already evidenced by Ashurov *et al.* a time ago [14]. Recent theoretical calculations show that creation of these defects in aluminum garnets is relatively easy [15]. The trap depth related to two dominant peaks at about 140 K and 165 K in LuAG:Ce was calculated to be about 0.31 eV and 0.38 eV, respectively. The dose dependence of the TSL glow curve confirmed the first order recombination process. Therefore detrapping times for both traps at RT could have been calculated and the values of about 50 μs and 450 μs, respectively, were obtained. Apparently, thermally induced detrapping from these traps into the conduction band followed by delayed radiative recombination at Ce^{3+} ions cannot explain the slower, submicrosecond component in the scintillation decay (Fig. 1). As spatially-correlated AD-Ce_{Lu} pairs were found with the help of EPR and tunneling recombination between related electron and hole trapped at such pairs was suggested at least within 10–40 K (region 1 in Fig. 2) [16], it seems reasonable to consider tunneling recombination process to explain also slower, submicrosecond decay component in the RT scintillation decay.

In the search for further optimization of LuAG-based scintillator a systematic attention was paid to reduce the trapping effects related to the Lu_{Al} AD electron trap. We found that Ga-admixed LuAG with the formula $Lu_3(Ga_{0.4}Al_{0.6})_5O_{12}$:Pr shows considerably lower TSL intensity and rather structureless TSL pattern shifted to lower temperatures with respect to LuAG:Pr [12]. Furthermore, its scintillation decay was significantly accelerated. Another set of samples with Ga relative content 0.05, 0.1 and 0.2 was prepared to study Ga-concentration dependence of trapping phenomena in Pr-doped Lu(Ga,Al)G host. While the host luminescence due to the AD defect was efficiently suppressed already at the lowest Ga concentration [17], TSL glow curve shows smooth shift to lower temperatures and lower intensities, Fig. 4. VUV excitation spectra measured for some of

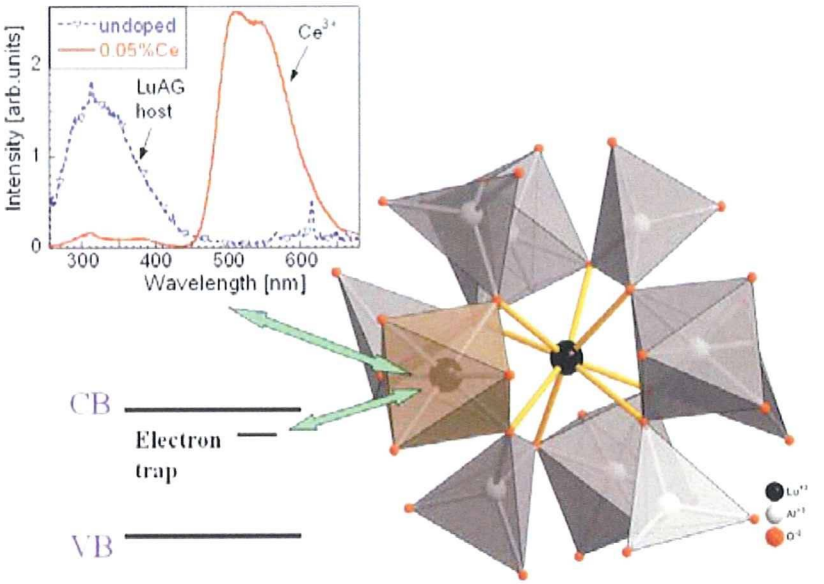

Fig. 3. The Lu_{Al} antisite defect in the LuAG structure. Resulting electron trap in the material forbidden gap is sketched on the left. Emission band within 300–350 nm due to antisite defect and its competition with that of the Ce^{3+} center can be derived from radioluminescence spectra at RT—upper left. Emission lines around 312 nm and 615 nm in the undoped sample are due to Gd^{3+} and Eu^{3+} accidental impurities, respectively.

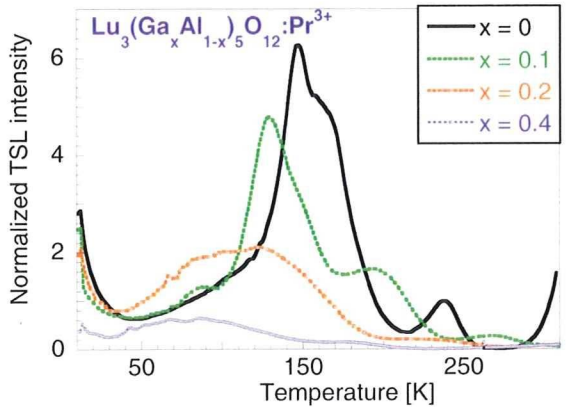

Fig. 4. TSL glow curves after x-irradiation at 10 K for Ga-admixed LuAG.

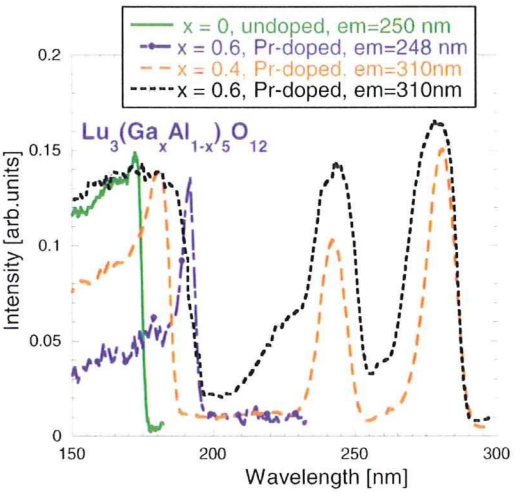

Fig. 5. Excitation spectra of undoped and Pr-doped $Lu_3(Ga_xAl_{1-x})_5O_{12}$ single crystals at 10 K.

these samples show a host band-edge shift towards lower energies. For the $Ga_{0.4}$ concentration it is of about 0.4 eV, which is comparable with the Lu_{Al} trap depth mentioned before, Fig. 5. TSL gradual change in Fig. 4 does not point to a 1:1 suppression of the Lu_{Al} defects due to the Ga admixture. Given the value of the band edge shift it rather seems that the levels of Lu_{Al} defects become gradually buried in the lowered bottom of the conduction band, which becomes dominated by the Ga wave functions.

Additional shift of the band edge towards lower energies for Ga admixture greater than 0.4 can be related to increasing occupancy of tetrahedral Al sites by Ga. Their energy levels are expected to be lower with respect to the garnet octahedral sites [18]. Despite the gradual acceleration of scintillation decay with increasing Ga content the light yield does not increase with respect to the Ga-free LuAG:Pr and overall radioluminescence intensity gets even lower, Fig. 6. This may indicate that Ga admixture induces additional nonradiative losses. Further systematic studies are needed to explain the observed characteristics.

B. *Ce-Doped Aluminum Perovskites*

Luminescence of $YAlO_3$:Ce (YAP:Ce) was reported by Weber [19], while the favourable properties of this material for scintillation applications were described later by Takeda *et al.* [20] and Autrata [21]. $LuAlO_3$:Ce became of interest in the mid nineties due to its higher density and effective atomic number [7], [22], [23] and later on also the mixed $Lu_xY_{1-x}AlO_3$:Ce crystals were prepared and characterized [24], [25]. A review paper devoted to this group of scintillation materials has been published recently [1].

The 370 nm emission of Ce^{3+} center in YAP shows a single-exponential fast PL decay with the decay time of about 17 ns. Somewhat longer scintillation decay time between 22 and 38 ns followed by a minor slower component with a decay time

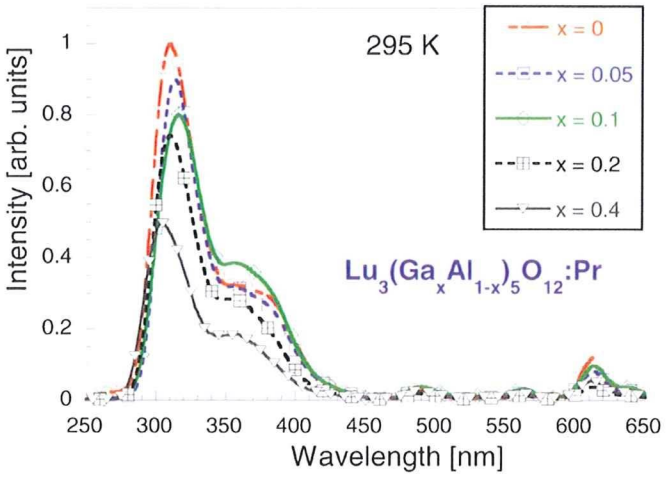

Fig. 6. Radioluminescence spectra at RT. Excitation by an X-ray tube, 40 kV.

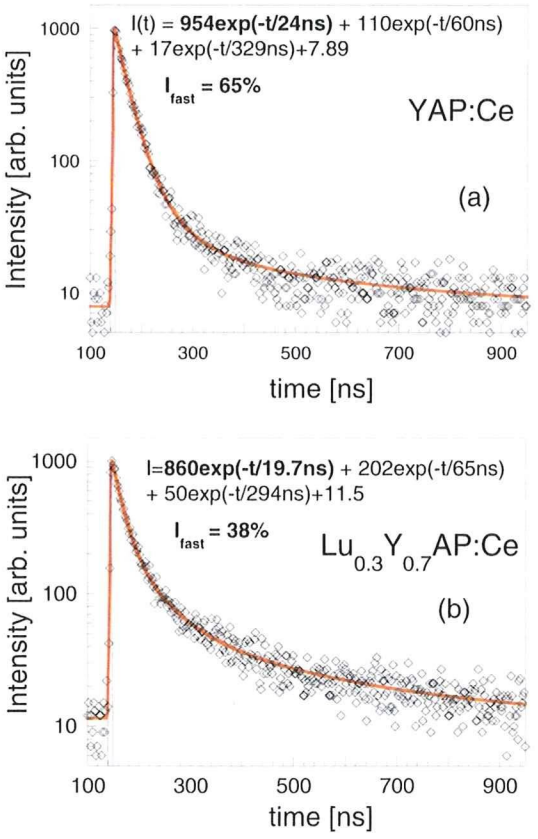

Fig. 7. Spectrally unresolved scintillation decays of LuAP:Ce (a) and LuYAP:Ce (b) excited by 511 keV of ^{22}Na radioisotope at RT.

of a few hundreds of nanoseconds is evaluated in the scintillation decay [26], [27]. The latter component can be explained by delayed recombination of charge carriers at Ce^{3+} centres (similarly as in aluminum garnets). The scintillation response of pure LuAP:Ce is dominated $\sim 80\%$ of the overall intensity) by a fast decay component of about 17–19 ns, while the rest of the intensity is released with a decay time of 160–180 ns.

In the case of Lu-rich mixed ($x = 0.65 - 0.7$) crystals, the intensity of the fast component is considerably reduced (40–54%) and, accordingly, the second slower component

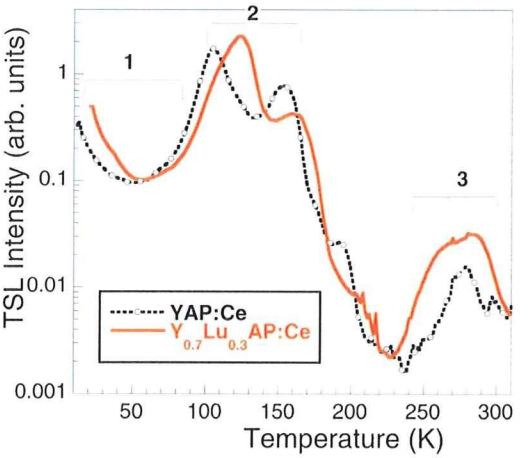

Fig. 8. TSL glow curves after irradiation at 10 K of YAP:Ce and LuYAP:Ce.

with the decay time of about 190 ns becomes more intense [28]. A comparison of scintillation decays of YAP:Ce and $Lu_{0.3}Y_{0.7}AlO_3$:Ce is given in Fig. 7(a) and (b). Apparently, there is an increase of the slower scintillation process and similar situation as in the Lu-rich $Lu_xY_{1-x}AlO_3$:Ce occurs. Thus, while the limit YAP:Ce and LuAP:Ce compositions show dominating fast emission component with the decay time of about 20 ns, the relative content of slower processes in the mixed compounds considerably increases. Fig. 8 displays the TSL glow curves of the above mentioned two samples after X-irradiation at 10 K. One can distinguish three typical regions in YAP:Ce (more than ten different YAP:Ce single crystals have been studied for TSL characteristics so far). Regions 1 and 2 resemble those found in YAG:Ce and within the region 1 the YAP:Ce phosphorescence decay exactly follows the t^{-1} form as shown in detail in [29]. It is interesting to note that based on comparison with the optical ceramics the 92 K glow curve peak in YAG:Ce was interpreted as due to the AD-related electron trap [30]. In the undoped and Ce-doped YAP the glow curve peak at around 150 K has been ascribed to the thermal decay of an O^- center [16]. The dose dependence of glow curves confirmed the first order TSL recombination kinetics of both 105 K and 150 K peaks. Therefore corresponding detrapping times at RT were easily calculated, yielding the values of about 100–200 μs [29]. Consequently, retrapping of migrating carriers at RT due to the traps related to the 105 K and 150 K glow-curve-peaks induces similar delays with respect to LuAG:Ce decribed earlier. However, one has to point out that relative intensity of TSL peaks in region 3 is much higher in LuAG:Ce, (see Fig. 2), than in YAP:Ce (Fig. 8). Much longer corresponding detrapping times at RT are expected, i.e., related traps in region 3 would have more detrimental effect on the time characteristics and light yield (LY) of such a scintillator.

Admixture of Lu into YAP:Ce results in the shift of the position of the dominant TSL peak up to about 125 K and to peak broadening, Fig. 8. Furthermore, relative intensity of TSL peaks in region 3 is enhanced. Whatever is the nature of related electron traps, the admixture of Lu into YAP:Ce is thus expected to slow down retrapping processes due to these traps, which may show a detrimental influence on the value of LY.